



## Light scattering from dense cold atomic media

Bihui Zhu, John Cooper, Jun Ye, and Ana Maria Rey

*JILA, NIST and University of Colorado, 440 UCB, Boulder, Colorado 80309, USA*  
*and Department of Physics, University of Colorado, 440 UCB, Boulder, Colorado 80309, USA*

(Received 20 May 2016; published 9 August 2016)

We theoretically study the propagation of light through a cold atomic medium, where the effects of motion, laser intensity, atomic density, and polarization can all modify the properties of the scattered light. We present two different microscopic models: the “coherent dipole model” and the “random-walk model”, both suitable for modeling recent experimental work done in large atomic arrays in the low-light-intensity regime. We use them to compute relevant observables such as the linewidth, peak intensity, and line center of the emitted light. We further develop generalized models that explicitly take into account atomic motion. Those are relevant for hotter atoms and beyond the low-intensity regime. We show that atomic motion can lead to drastic dephasing and to a reduction of collective effects, together with a distortion of the line shape. Our results are applicable to model a full gamut of quantum systems that rely on atom-light interactions, including atomic clocks, quantum simulators, and nanophotonic systems.

DOI: [10.1103/PhysRevA.94.023612](https://doi.org/10.1103/PhysRevA.94.023612)

### I. INTRODUCTION

Light-matter interactions are fundamental for the control and manipulation of quantum systems. Thoroughly understanding them can lead to significant advancements in quantum technologies, quantum simulations, quantum information processing, and precision measurements [1–7]. Over the past decades, cold-atom experiments have provided a clean and tunable platform for studying light-matter interactions in microscopic systems where rich quantum effects emerge, such as superradiance and subradiance, electromagnetically induced transparency, and nonclassical states of light [8–12]. However, in spite of intensive theoretical and experimental efforts over the years, long-standing open questions still remain regarding the propagation of light through a coherent medium, especially when it consists of large and dense ensembles of scatterers [13–29]. In fact, by studying small systems where analytical solutions are obtainable, it has been realized that atom-atom interactions can significantly modify the spectral characteristics of the emitted light. These effects yet need to be understood in large systems [30–34] where finite-size effects and boundary conditions become irrelevant. The situation is even more complicated when the coupling with atomic motion is non-negligible [35,36]. It is timely to develop theories capable of addressing these questions, given the rapid developments on cold-atom experiments and nanophotonic systems. The experiments are entering strongly coupled regimes, where atom-atom and atom-photon interactions need to be treated simultaneously and sometimes fully microscopically [30,37,38].

A widely adopted approach to describe light scattering consists of integrating out the atomic degrees of freedom and treating the atoms just as random scatterers with prescribed polarizability [39–42]. While this approach can successfully capture some classical properties of the scattered light, it does not fully treat the roles of atom-atom interactions and atomic motion [43–46]. An alternative route consists of tracing over the photonic degrees of freedom. In this case the virtual exchange of photons induces dispersive and dissipative dipole-dipole interactions between atoms, which can be accounted for

by a master-equation formulation [13,14]. This approach has been used to study systems of tightly localized atoms where the dynamics only takes place in the atomic internal degrees of freedom. It has been shown to successfully capture quantum effects in light scattering [18,19,47–50]. However, due to the computational complexity, it has been often restricted to weak excitation and small samples [32,33,51,52], and a direct comparison with experiments containing a large number of atoms has been accomplished only recently [53,54]. In general, most theories have not properly accounted for atomic motional effects and atomic interactions on the same footing and many open questions in light-scattering processes remain.

Here, we present a unifying theoretical framework based on a coherent dipole (CD) model [see Fig. 1(a)] to study the light scattering from cold atoms with possible residual motion. In the low-intensity and slow-motion regime, we use the CD to investigate the collective effects in the light scattered by a large cloud and show the interplay of optical depth (OD) and density. These results are compared with the random-walk (RW) model [see Fig. 1(a)] that only accounts for incoherent scattering and thus ignores coherent dipolar interaction effects. To address the role of atomic motion, we perform different levels of generalization of the CD model. With these modified models, we show that atomic motion not only reduces phase coherence and collective effects but also impacts the line shape and line center of the spectral emission lines via photon recoils. Motivated by a recent experiment at the Joint Institute for Laboratory Astrophysics (JILA) [see Fig. 1(b)] [53], we focus our discussions on a  $J = 0 \rightarrow J' = 1$  transition, but the methods presented here can be extended to more complicated level structures without much difficulty.

This paper is organized as follows. In Sec. II, we provide the mathematical description of the CD model, which treats atoms as coupled, spatially fixed dipoles sharing a single excitation. Its predictions on the collective properties of the emitted light such as the light polarization and density dependence of the line shape and peak intensity are discussed. In Sec. III, we introduce the RW model and compare its predictions on the linewidth and peak intensity of the scattered light to the ones obtained from the CD model. Those comparisons allow us to

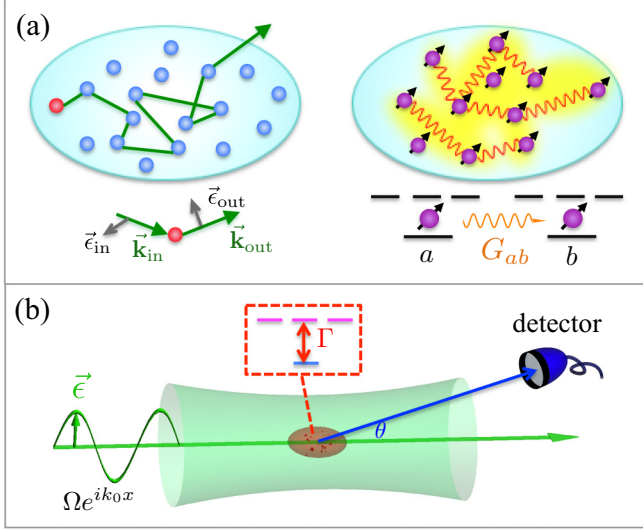


FIG. 1. Scheme. (a) Microscopic models: random-walk model (left) and coherent dipole model (right). In the random-walk model, a photon is randomly scattered by the atoms. Scattering events are characterized by the incident and outgoing wave vectors of the photons and their corresponding polarizations. In the coherent dipole model, atoms are coupled by dipole-dipole interactions  $G_{ab}$ , and all atoms contribute to the fluorescence. (b) Experimental setup for measuring the fluorescence from a cloud of atoms. An incident laser drives an atomic transition with a spontaneous emission rate  $\Gamma$ . Atoms absorb and emit light. The detectors collect scattered photons at an angle  $\theta$  measured from the incident beam direction.

explore the role of phase coherence in the atom-light interaction. In Sec. IV, we present extended models to study motional effects on atomic emission. We first include motion in the CD model by assuming that its leading contributions comes from Doppler shifts. Those are accounted for in the frozen model approximation when we introduce local random detunings for atoms sampled from a Maxwell-Boltzmann distribution. Then we go beyond the frozen model approximation and explicitly include atomic motion by means of a semiclassical approach. This treatment also allows us to go beyond the low-excitation regime. We finish in Sec. V with conclusions and an outlook.

## II. COHERENT DIPOLE MODEL

### A. Equations of motion for coherent dipoles

For an ensemble of  $N$  atoms with internal dipole transition  $J = 0 \rightarrow J' = 1$ , the Hamiltonian of the system that includes the interaction between atoms and the radiation field is [55]

$$H = \hbar \sum_{\mathbf{k}, \epsilon} \omega_{\mathbf{k}} \hat{a}_{\mathbf{k}\epsilon}^\dagger \hat{a}_{\mathbf{k}\epsilon} + \hbar \sum_{i, \alpha} \omega_{\alpha} \hat{b}_i^{\alpha\dagger} \hat{b}_i^{\alpha} + \sum_i \hat{\mathbf{D}}_i \cdot \hat{\mathbf{E}}(\mathbf{r}), \quad (1)$$

$$\hat{D}_i^{\alpha} = d(\hat{b}_i^{\alpha\dagger} + \hat{b}_i^{\alpha}), \quad (2)$$

$$\hat{\mathbf{E}}(\mathbf{r}) = \sum_{\mathbf{k}\epsilon} g_{\mathbf{k}} \epsilon_{\mathbf{k}} (e^{i\mathbf{k}\cdot\mathbf{r}} \hat{a}_{\mathbf{k}\epsilon} + \text{H.c.}), \quad (3)$$

where we have used the notation  $|\alpha\rangle$  to denote the excited levels and  $|0\rangle$  for the lower state. For convenience, we choose the Cartesian basis,  $|\alpha\rangle = |x\rangle, |y\rangle, \text{ or } |z\rangle$ .  $\hat{b}_i^{\alpha\dagger} = |\alpha\rangle_i \langle 0|_i$  is the

raising operator for transition to state  $|\alpha\rangle$  of the  $i$ th atom, and  $d$  is the atomic dipole moment. The field coupling strength is denoted by  $g_{\mathbf{k}} = \sqrt{\frac{\hbar\omega_{\mathbf{k}}}{2\epsilon_0 V}}$ ,  $\mathbf{k}(\epsilon)$  is the wave vector (polarization) of the photons,  $\omega_{\mathbf{k}}$  is the frequency of the photons,  $\epsilon_0$  is the vacuum permittivity, and  $V$  is the photon quantization volume. Under the Born-Markov approximation, the photon degrees of freedom  $\hat{a}_{\mathbf{k}\epsilon}$  can be adiabatically eliminated, leading to a master equation for the reduced density matrix  $\hat{\rho}$  of the atoms [13,30,55] where the effective role of the scattered photons is to mediate dipole-dipole interactions between atoms. The master equation for  $\hat{\rho}$  is

$$\begin{aligned} i \frac{d\hat{\rho}}{dt} = & - \sum_{i, \alpha} \Delta^{\alpha} [\hat{b}_i^{\alpha\dagger} \hat{b}_i^{\alpha}, \hat{\rho}] + \sum_{i, \alpha} \Omega^{\alpha} [(e^{i\mathbf{k}_0 \cdot \mathbf{r}_i} \hat{b}_i^{\alpha\dagger} + \text{H.c.}), \hat{\rho}] \\ & + \sum_{i \neq j, \alpha, \alpha'} g_{i, j}^{\alpha\alpha'} [\hat{b}_i^{\alpha\dagger} \hat{b}_j^{\alpha'}, \hat{\rho}] \\ & + \sum_{i, j, \alpha, \alpha'} f_{i, j}^{\alpha\alpha'} (2\hat{b}_j^{\alpha'} \hat{\rho} \hat{b}_i^{\alpha\dagger} - \{\hat{b}_i^{\alpha\dagger} \hat{b}_j^{\alpha'}, \hat{\rho}\}), \end{aligned} \quad (4)$$

where we have added the term describing the effect of an external driving laser with polarization  $\alpha$ , wave vector  $\mathbf{k}_0$ , and Rabi frequency  $\Omega^{\alpha}$ . The Hamiltonian is written in the rotating frame of the laser, with  $\Delta^{\alpha}$  denoting the detuning between the laser and the transition  $|0\rangle \rightarrow |\alpha\rangle$ . The dipole-dipole interactions are given by [13,30]

$$G_{ij}^{\alpha\alpha'} = \frac{3\Gamma}{4} [\delta_{\alpha, \alpha'} A(r_{ij}) + \hat{\mathbf{r}}_{ij}^{\alpha} \hat{\mathbf{r}}_{ij}^{\alpha'} B(r_{ij})], \quad (5)$$

$$A(r) = -\frac{e^{ik_0 r}}{k_0 r} - i \frac{e^{ik_0 r}}{k_0^2 r^2} + \frac{e^{ik_0 r}}{k_0^3 r^3}, \quad (6)$$

$$B(r) = \frac{e^{ik_0 r}}{k_0 r} + 3i \frac{e^{ik_0 r}}{k_0^2 r^2} - 3 \frac{e^{ik_0 r}}{k_0^3 r^3}, \quad (7)$$

$$g_{ij}^{\alpha\alpha'} = \text{Re}[G_{ij}^{\alpha\alpha'}], \quad (8)$$

$$f_{ij}^{\alpha\alpha'} = \text{Im}[G_{ij}^{\alpha\alpha'}], \quad (9)$$

where  $\delta_{\alpha, \alpha'}$  is the Kronecker delta symbol,  $\mathbf{r}_{ij}$  is the relative separation between atoms  $i$  and  $j$ , and  $\hat{\mathbf{r}}^{\alpha} = \mathbf{r}^{\alpha}/r$  denotes the component of the unit vector  $\mathbf{r}/r$  along the direction  $\alpha = x, y, \text{ or } z$ . The real and imaginary parts describe the dispersive and dissipative interactions, respectively. The spontaneous emission rate is  $\Gamma = \frac{k_0^3 d^2}{3\pi\hbar\epsilon_0}$ , and  $k_0 = 2\pi/\lambda$  is the wave vector of the dipole transition. The dipole-dipole interactions include both the far-field ( $1/r$ ) and near-field ( $1/r^2, 1/r^3$ ) contributions. The imaginary part encapsulates the collective dissipative process responsible for the superradiant emission in a dense sample. The real part accounts for elastic interactions between atoms which can give rise to coherent dynamical evolution. These elastic interactions compete with and can even destroy the superradiant emission [33,56].

When the atoms' thermal velocity  $v$  satisfies  $k_0 v \ll \Gamma$ , atoms can be assumed to be frozen during the radiation process. Moreover, in the weak-driving regime,  $\Omega \ll \Gamma$ , to an excellent approximation, the master-equation dynamics can be captured by the  $3N$  linear equations describing the atomic coherences  $b_j^{\alpha} = \langle \hat{b}_j^{\alpha} \rangle$  of an excitation propagating through the ground-state atomic medium. The corresponding steady-state

solution can be found from

$$b_j^\alpha = \frac{\Omega^\alpha \delta_{\alpha,\gamma} e^{i\mathbf{k}_0 \cdot \mathbf{r}_j} / 2}{\Delta^\alpha + i\Gamma/2} + \sum_{n \neq j, \alpha'} \frac{G_{jn}^{\alpha\alpha'}}{\Delta^\alpha + i\Gamma/2} b_n^{\alpha'}, \quad (10)$$

where we have specified the polarization of the driving laser to be along  $\gamma$ . To obtain Eq. (10), we have assumed there is only one excitation in the system and ignored multiatom coherences (see Appendix A). This assumption is justified in the weak-driving-field regime [49,57]. The fluorescence intensity measured at the position  $\mathbf{r}_s$  in the far field can be obtained by the summation [13]

$$I(\mathbf{r}_s) \propto \sum_{jn} e^{-i\mathbf{k}_s \cdot \mathbf{r}_{jn}} \sum_{\alpha, \alpha'} (\delta_{\alpha, \alpha'} - \hat{\mathbf{r}}_s^\alpha \hat{\mathbf{r}}_s^{\alpha'}) b_j^\alpha b_n^{\alpha*}, \quad (11)$$

where  $b_n^{\alpha*}$  is the complex conjugate of  $b_n^\alpha$ , and  $\mathbf{r}_{jn} = \mathbf{r}_j - \mathbf{r}_n$ .

### B. Collective effects in fluorescence

For dilute samples the dipolar interactions are weak,  $\mathcal{G} \equiv \sum_{i \neq j, \alpha, \alpha'} |G_{ij}^{\alpha\alpha'}| / (N\Gamma) \ll 1$ , and Eq. (10) can be solved perturbatively using  $\mathcal{G}$  as an expansion parameter,  $b_j^\alpha = b_j^{\alpha,0} + b_j^{\alpha,1} + b_j^{\alpha,2} + \dots$  ( $b_j^{\alpha,n} \propto \mathcal{G}^n$ ), which results in

$$b_j^{\alpha,n} = \sum_{\substack{l_1 \neq j \\ l_2 \neq l_1 \\ \dots l_n \neq l_{n-1} \\ \alpha_1, \alpha_2, \dots, \alpha_n}} \frac{G_{jl_1}^{\alpha\alpha_1} G_{l_1 l_2}^{\alpha_1 \alpha_2} \dots G_{l_{n-1} l_n}^{\alpha_{n-1} \alpha_n} \Omega^\gamma \delta_{\alpha_n, \gamma} e^{i\mathbf{k}_0 \cdot \mathbf{r}_{jn}}}{i^n (\Delta^\alpha + i\frac{\Gamma}{2}) (\Delta^{\alpha_1} + i\frac{\Gamma}{2}) \dots (\Delta^{\alpha_n} + i\frac{\Gamma}{2})}. \quad (12)$$

In the expansion, terms of order  $n$  account for  $n$ th-order scattering events. For simplicity, in the following we assume the atomic sample has a spherical shape, with density distribution  $n(r) = n_0 e^{-r^2/2R^2}$ , unless otherwise specified. However, the conclusions can be generalized to other geometries. Here,  $n_0 = \frac{N}{2\pi\sqrt{2\pi}R^3}$  is the peak density.

To the zeroth order, the atomic response is driven by only the external field and is not modified by the scattered light:

$$b_j^{\alpha,0} = \frac{\Omega^\alpha \delta_{\alpha,\gamma} e^{i\mathbf{k}_0 \cdot \mathbf{r}_j}}{\Delta^\alpha + i\Gamma/2}. \quad (13)$$

Substituting it into Eq. (11), the intensity of scattered light is

$$I \propto N + N^2 e^{-|\mathbf{k}_s - \mathbf{k}_0|^2 R^2}. \quad (14)$$

There are two contributions to the intensity; the first term  $\propto N$  represents the incoherent contribution, and the second term  $\propto N^2$  is the collective emission resulting from coherent scattering processes [17,53]. The phase coherence is restricted to a narrow angular region around the incident laser direction, with  $\delta\theta \sim 1/k_0 R$ . The enhanced emission arises from the constructive interference of the radiation from  $N$  dipoles [49]. Along other directions, the random distribution of atom positions randomizes the phases of the emitted light, smearing out the phase coherence after averaging over the whole sample [53].

Including first-order corrections, the intensity of the scattered light is given by

$$I(r_s) \propto \frac{N\Omega^2}{(\Delta - \Gamma\text{Re}[\bar{G}])^2 + (\Gamma + 2\Gamma\text{Im}[\bar{G}])^2/4} \quad (15)$$

for transverse directions, where we have denoted  $\Omega = \Omega^\gamma$  and  $\Delta = \Delta^\gamma$  and  $\bar{G} = \sum_{i \neq j} G_{ij}^{\gamma\gamma} e^{-i\mathbf{k}_0 \cdot \mathbf{r}_{ij}} / (N\Gamma)$ . For the forward direction, the intensity has the same form, except that the factor  $N$  is replaced by  $N^2$  due to the phase coherence. Therefore, the line shape of the scattered light is Lorentzian, with its line-center frequency shifted by the elastic interactions [58] and the linewidth broadened by the radiative interactions. If we temporarily neglect the effect of polarization, when the atom-atom separation is large, the dipole-dipole interaction is dominated by far-field terms, i.e.,  $G_{ij}^{\gamma\gamma} \sim -\frac{3\Gamma}{4} (1 - \hat{\mathbf{r}}_{ij}^\gamma \hat{\mathbf{r}}_{ij}^\gamma) \frac{e^{ik_0 r_{ij}}}{k_0 r_{ij}}$ . In this limit analytical expressions for the linewidth broadening  $\bar{\Gamma}$  and density shift  $\bar{\Delta}$  can be obtained:  $\bar{\Gamma} = 2\Gamma\text{Im}[\bar{G}] = 3N\Gamma/(8k_0^2 R^2) = \frac{\tau}{4}\Gamma$ , with  $\tau = \frac{3N}{2k_0^2 R^2}$  being the OD of the sample (see Appendix B), and  $\bar{\Delta} = \Gamma\text{Re}[\bar{G}] = -\Gamma n_0 k_0^{-3} / 4\sqrt{2\pi}$ . Therefore, while the collectively broadened linewidth depends on the OD of the atomic cloud, the frequency shift depends on the density.

In a dense medium dipolar interactions are strong,  $\mathcal{G} \gtrsim 1$ , higher-order scattering events become important, and the interplay between the radiative interactions and elastic interactions becomes non-negligible. As a consequence the above perturbative analysis is no longer applicable. In Figs. 2 and 3, we show the numerical solution of Eq. (10), which takes into account all the scattering orders. As shown in Fig. 2(a), most of the scattered light is distributed within a narrow peak around the forward direction (laser direction). Outside this narrow region fluorescence is almost uniformly distributed among other directions [59]. The forward emission is collectively enhanced. For low OD it increases as  $\sim N^2$  [Fig. 2(b)], while the transverse intensity increases as  $\sim N$ .

Dipolar interactions tend to suppress the rate at which the intensity grows with  $N$  [Fig. 2(c)]. This can be qualitatively understood from Eq. (15), which predicts that the intensity is reduced as OD increases. Despite the fact that the perturbative analysis is only valid in the weak-interaction limit, this tendency remains and becomes more pronounced in the large-OD regime, as shown by the numerical solution presented in Fig. 2(d). Broadly speaking, multiple-scattering events tend to suppress collective behavior [22,60]. Similar physics is also observed in the behavior of the linewidth. At small OD, the FWHM linewidth increases linearly with OD [Fig. 3(a)], and the line shape is well described by a Lorentzian [Fig. 3(b)], as expected from Eq. (15). However, when OD is large and the density is high, in addition to a significant broadening, the line shape becomes non-Lorentzian [Fig. 3(c)], and the FWHM increases slowly with OD [Fig. 3(a)]. To further illustrate this, in Fig. 3(a) we plot the FWHM for the same OD but with smaller density (by using a larger atom number). The figure shows that the linewidth indeed keeps increasing until saturation at a larger value of OD. Another interesting feature is the double-peak structure observed only at intermediate angles  $\theta$ , which arises from the interplay between the stimulated photon emission driven by the probe field and the scattered photons emitted via dipolar exchange processes [Fig. 3(c)].

The drastic modifications of the perturbative expectations from multiple scattering are also present in the frequency shift of the scattered light. From a mean-field point of view, the line center of scattered light is shifted according to the Lorentz-Lorenz shift  $\pi n_0 k_0^{-3} \Gamma$  [61]. As shown by the

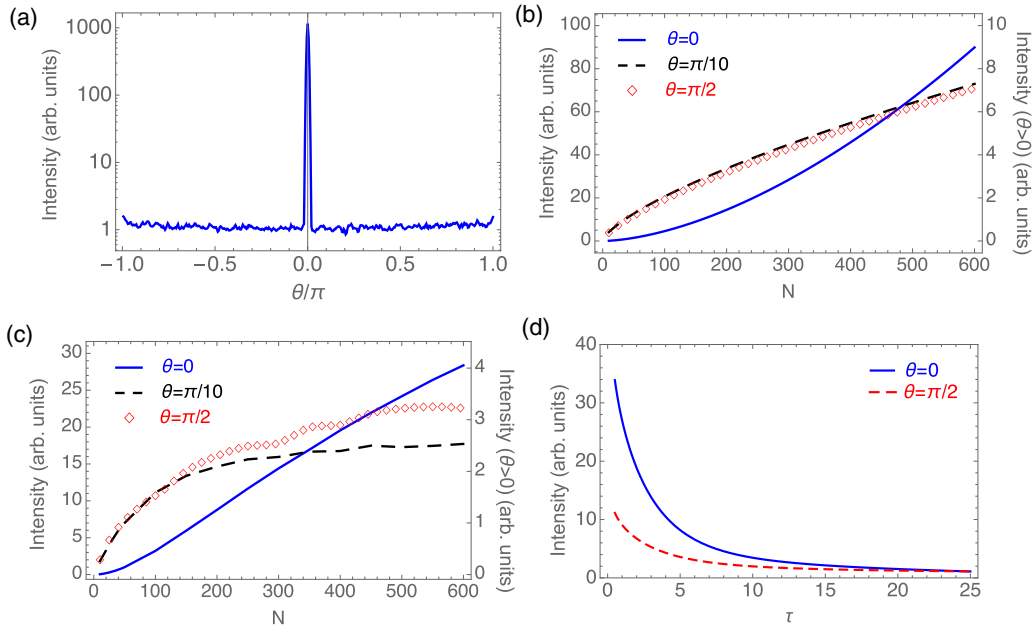


FIG. 2. CD model: on-resonance intensity. (a) Angular distribution: due to the constructive interference along the forward direction ( $\theta = 0$ ), the intensity is drastically enhanced within a small angular region. (b) and (c) The intensities for three different directions ( $\theta = 0, \pi/10, \pi/2$ ) are shown as a function of atom number, each normalized to the value at  $N = 50$ . All are calculated for a spherical cloud of fixed size. The right vertical axes label the intensity for  $\theta = \pi/2, \pi/10$ . In (b) the OD and the density are relatively low (when  $N = 500$ ,  $\tau = 2$ ,  $n_0 k_0^{-3} = 0.0015$ ). The transverse intensity increases  $\sim N$ , while the forward intensity increases  $\sim N^2$ , showing a collective enhancement for a small window of  $\theta$  around zero. Outside this narrow angular window the enhancement disappears, and the intensity becomes almost  $\theta$  independent, as indicated by the identical behavior observed for two different angles,  $\theta = \pi/10$  and  $\pi/2$ . In (c) the OD and density are relatively large (when  $N = 500$ ,  $\tau = 10$ ,  $n_0 k_0^{-3} = 0.017$ ). The rate at which the intensity increases with  $N$  slows down in both the forward and transverse directions, with  $I \sim N^1$  for  $\theta = 0$  and  $I \sim N^{0.5}$  for  $\theta = \pi/2$ , respectively. (d) On-resonance intensity as a function of OD: it is highly suppressed at large OD. Here, the intensity is normalized to the corresponding value at  $\tau = 25$  for each direction.

numerical calculation in Fig. 4 (blue solid line), at small density, the frequency shift is indeed linear with  $n_0 k_0^{-3}$ , but as density increases, the shift is quickly suppressed [22]. For atom density  $\sim 5 \times 10^{13} \text{ cm}^{-3}$  (reached, for example, in cold  $^{87}\text{Rb}$  atom experiments [62]), the calculated density shift is approximately a factor of 2 lower than the mean-field prediction.

The interplay between the imaginary and real parts of the dipole-dipole interaction has to be carefully accounted for to compare numerical simulations with experimental measurements by doing finite-size scaling. For typical computation resources the numerical solution of Eq. (10) is limited to  $\sim 10^4$  atoms. On the other hand, experiments usually operate with ensembles of tens of millions of atoms. To theoretically model these large systems a proper rescaling in the cloud size is necessary. Equation (15) implies that in order to characterize the effect of radiative interactions one should aim to match the experimental OD, which scales as  $\sim N^{1/2}$ . On the other hand, to properly reproduce the effect of elastic interactions it is better to match the dimensionless number  $n_0 k_0^{-3}$ , which scales as  $N^{1/3}$ . Therefore, there exist two different ways of rescaling the cloud size, either by keeping the same OD or the same density. In Fig. 5 we show the effect of finite  $N$  for a moderate range of atom numbers. Indeed, except from small deviations seen at very low atom numbers ( $< 1000$ ), the linewidth broadening can be well captured by keeping the OD constant, while the frequency shift is well described by using a constant density. In contrast, if a constant OD is used to compute the frequency

shift, the result would considerably overestimate the shift, e.g., by a factor of 10 when the  $N$  in numerical simulation is 1/100 the atom number in experiment. The interplay of multiple scattering and density effects is more prominent for larger  $N$  values. To deal with the OD vs density scaling issues in comparing with experiments the most appropriate rescaling procedure that we found is the following: when computing the linewidth or peak intensity, the theory is rescaled accordingly with the experimental OD. However, the actual OD value is not exactly matched to the experimental one but to a slightly modified value,  $\tilde{\tau} = \eta \tau$  to account for density effects [53]. For a moderate window of OD values, for example, achieved experimentally by letting the cloud expand for different times,  $\eta$  should be kept fixed. For the frequency shift the theory should be rescaled according to density.

### C. Anisotropic features of scattered light

For independent atoms radiation along the polarization of the driving laser is forbidden. However, dipole-dipole interactions can generate polarization components different from the driven ones if the atoms exhibit internal level structure, e.g., degenerate Zeeman levels in the excited state. This is the case of a  $J = 0 \rightarrow J' = 1$  transition, where, as shown in Fig. 6, the fluorescence emitted along the laser polarization direction ( $z$  direction,  $\theta = \pi/2$ ) is nonzero. It is, however, much weaker than the intensity emitted along other directions. On the contrary, for two-level transitions

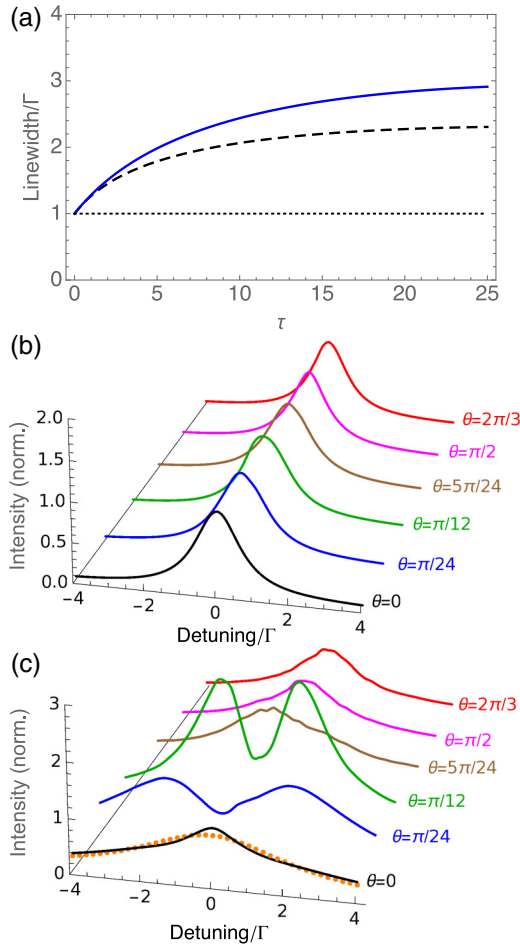


FIG. 3. CD model: collective broadening. (a) FWHM linewidth as a function of OD. At small OD, the FWHM increases linearly with OD, but as OD increases, density effects set in, multiple scattering events become relevant, and the linewidth dependence on OD is no longer linear. Two different atom numbers are used for the blue solid ( $N = 1000$ ) and black dashed ( $N = 200$ ) lines, and the OD is varied by changing the cloud size. For the blue solid line,  $n_0 k_0^{-3} = 0.14$  at  $\tau = 25$  and  $0.003$  at  $\tau = 2$ . For the black dashed line, the density at the same OD is doubled. With smaller density, the linewidth increases to a larger value in the large-OD regime. (b) The line shape at small OD values ( $\tau = 2$ ,  $n_0 k_0^{-3} = 0.002$ ) for different angles  $\theta$  [ $\theta$  is defined in Fig. 1(a)] is mainly Lorentzian. Here, the intensity is normalized to the on-resonance intensity for each  $\theta$ . (c) At large OD ( $\tau = 20$ ,  $n_0 k_0^{-3} = 0.06$ ), the fluorescence line shape significantly broadens and stops being Lorentzian. The brown dots for  $\theta = 0$  show the Lorentzian fit, which fails to describe the line shape. At intermediate  $\theta$ , a double-peak structure shows up. For all panels, the cloud shape is spherical.

the polarization of the scattered light is conserved, and thus, the emission parallel to the laser polarization is completely suppressed. The strong dependence of the scattered light on polarization and atomic internal structure is most relevant along the transverse direction. Along the forward direction those effects are irrelevant, as verified by our numerical simulations. From Eq. (12), the lowest-order contribution to the intensity detected along the laser polarization direction comes from the first-order scattering processes; thus,  $I \propto \frac{1}{(\Delta^2 + \Gamma^2/4)^2}$ , which leads to a “subradiant” line shape (i.e., the

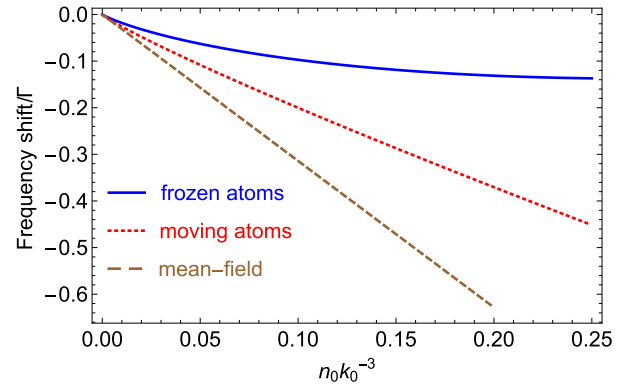


FIG. 4. CD model: frequency shift. For small density, the shift calculated from the coherent dipole model (blue solid line) increases linearly with density as predicted by the mean-field theory. However, when density is large, there is a significant deviation from the mean-field result. When motional effects are taken into account (red dotted line, Doppler width of  $5\Gamma$ , see Sec. IV A), the nonlinear suppression of the frequency shift with density is less severe.

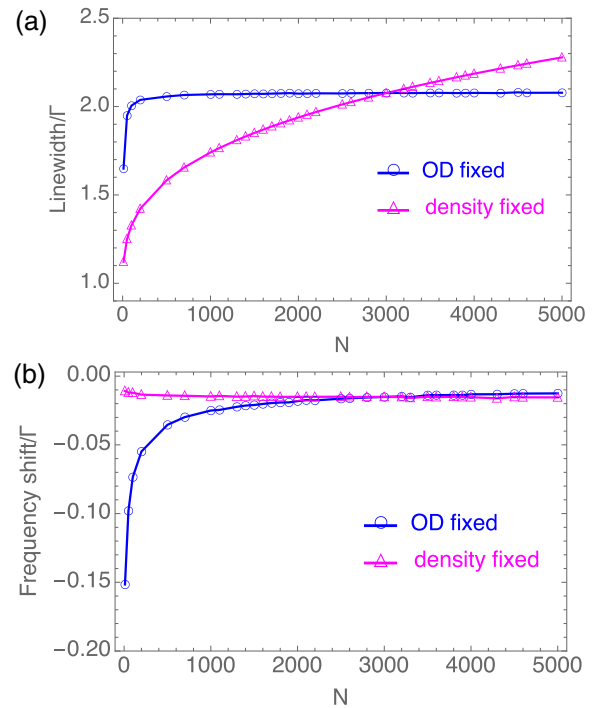


FIG. 5. CD model: finite-size scaling. (a) The linewidth is calculated for different numbers of atoms at the same OD ( $\tau = 4$  for  $N = 3000$ ) by varying the density (blue line with circles). From  $N = 1000$  to  $5000$  the linewidth is not obviously changed. In contrast, by keeping the same density ( $n_0 k_0^{-3} = 0.0037$  for  $N = 3000$ ) while varying the OD (magenta line with triangles), the linewidth keeps changing. (b) The frequency shift is calculated for different numbers of atoms. By keeping constant density (magenta line with triangles), the frequency shift remains almost constant, while for constant OD (blue line with circles), there is a significant variation of the frequency shift with  $N$ . Here, the cloud aspect ratio is  $R_x : R_y : R_z = 2 : 2 : 1$  [53].

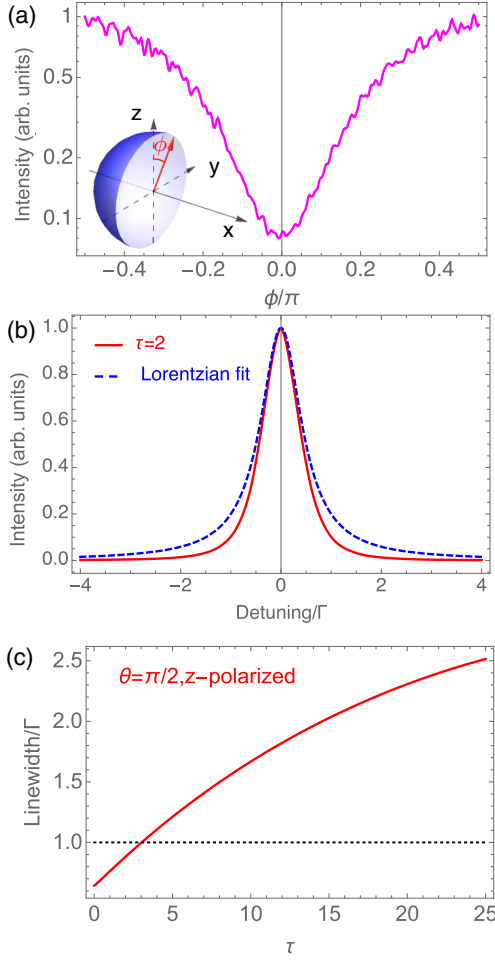


FIG. 6. CD model: effect of laser polarization. (a) Intensity distribution in the plane perpendicular to the laser propagation direction, i.e.,  $\theta = \pi/2$  for all  $\phi$ 's (inset shows the geometry).  $\phi = 0$  is the  $z$  direction. Here, the incident laser is polarized along  $z$ . The intensity detected along the laser polarization is suppressed compared to other directions. (b) and (c) show the line shape and linewidth of light detected at  $\theta = \pi/2$ ,  $\phi = 0$ . (b) At small OD, the FWHM linewidth is below the natural linewidth. (c) As OD increases, the linewidth is collectively broadened due to multiple-scattering processes [Fig. 3(a)]. For all panels, degeneracy in excited levels has been assumed.

FWHM,  $\bar{\Gamma}_{\text{FWHM}} = \sqrt{\sqrt{2} - 1}\Gamma < \Gamma$ , is smaller than the one for independent particles). The analytic result agrees perfectly with the numerical simulation at low OD [Fig. 6(b)]. As the OD increases and interactions become stronger, higher-order scattering contributions lead to a collective broadening (linewidth larger than  $\Gamma$ ) even along this “single-dipole-forbidden” direction, as shown in Fig. 6(c).

### III. RANDOM-WALK MODEL

In this section we use the random-walk model to investigate the role of incoherent scattering processes in collective emission. We focus on the low-intensity regime. Classically, light transport in a disordered medium can be described by a sequence of random scattering events experienced by a

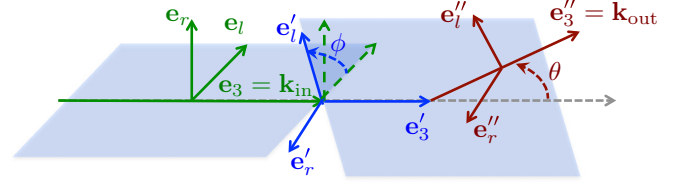


FIG. 7. RW: transformation of Stokes vectors. In the random-walk model, a scattering event is determined by two consecutive transformations of local coordinates:  $\{e_3, e_r, e_l\} \rightarrow \{e'_3, e'_r, e'_l\}$  via rotation  $\phi$  and  $\{e'_3, e'_r, e'_l\} \rightarrow \{e''_3, e''_r, e''_l\}$  via rotation  $\theta$  [68].

photon [see Fig. 1(a)] [41,44,60]. The expected number of scattering events is roughly given by  $(\tau_p)^2$ , where  $\tau_p$  is the peak optical depth, which depends on detuning  $\Delta$  as  $3N/[k_0^2 R^2(1 + 4\Delta^2/\Gamma^2)]$ . For simplicity here we also assume a spherical cloud. The transmission of light is given by  $e^{-\tau_p}$  [63,64]. For the  $J = 0 \rightarrow J' = 1$  transition (degenerated  $J' = 1$  states), the differential scattering cross section that defines a scattering event is given by [41,60]

$$\frac{d\sigma}{d\Omega}(\mathbf{k}_{\text{in}}, \epsilon_{\text{in}} \rightarrow \mathbf{k}_{\text{out}}, \epsilon_{\text{out}}) = \frac{3\sigma_0}{8\pi} |\epsilon_{\text{in}}^* \cdot \epsilon_{\text{out}}|^2, \quad (16)$$

where  $\mathbf{k}_{\text{in},\text{out}}$  are the incident and scattered wave vectors,  $\epsilon_{\text{in},\text{out}}$  are the polarizations of the incident and scattered photons [41,60,65], and  $\sigma_0 = 3\lambda^2/[2\pi(1 + 4\Delta^2/\Gamma^2)]$ , with  $\lambda$  being the wavelength of the driving laser.

To simulate the polarization-dependent scattering events as dictated by Eq. (16), it is convenient to use the Stokes-Mueller formalism [66]. A photon in a given state of polarization can be described by a Stokes vector [67]

$$\mathbf{S} = \begin{pmatrix} S_0 \\ S_1 \\ S_2 \\ S_3 \end{pmatrix} = \begin{pmatrix} |E_l|^2 + |E_r|^2 \\ |E_l|^2 - |E_r|^2 \\ E_l^* E_r + E_l E_r^* \\ i(E_l^* E_r - E_l E_r^*) \end{pmatrix}, \quad (17)$$

where  $E_l, E_r$  are the electric field components projected onto the two orthogonal axes  $\hat{e}_l$  and  $\hat{e}_r$  in the plane perpendicular to the wave vector  $\mathbf{k}$ . For example,  $\mathbf{S} = (1, 1, 0, 0)$  represents a photon linearly polarized along the reference axis  $\hat{e}_l$ . A scattering event  $\mathbf{k}_{\text{in}}, \epsilon_{\text{in}} \rightarrow \mathbf{k}_{\text{out}}, \epsilon_{\text{out}}$  can be determined by two angles:  $\theta$  and  $\phi$  (see Fig. 7). The change of polarization can be obtained from the transformation  $\mathbf{S}'' = M(\theta)\mathcal{R}(\phi)\mathbf{S}^{\text{in}}$ , where  $\mathbf{S}^{\text{in}}$  is the incident Stokes vector,  $\mathbf{S}''$  is defined with respect to the axes  $\hat{e}'_l, \hat{e}'_r$ , and  $\hat{e}'_3$ , and then  $\mathbf{S}^{\text{out}} = \mathcal{R}(\psi)\mathbf{S}''$ , transforming back to the original frame  $\hat{e}_l, \hat{e}_r$ , and  $\hat{e}_3$  [68], with  $\mathbf{S}^{\text{out}}$  being the scattered Stokes vectors. The scattering matrix that we use,  $M$ , is the scattering matrix that describes Rayleigh scattering [60,66]. It is given by

$$M(\theta) = \frac{3}{4} \begin{pmatrix} \cos^2\theta + 1 & \cos^2\theta - 1 & 0 & 0 \\ \cos^2\theta - 1 & \cos^2\theta + 1 & 0 & 0 \\ 0 & 0 & 2\cos\theta & 0 \\ 0 & 0 & 0 & 2\cos\theta \end{pmatrix}. \quad (18)$$

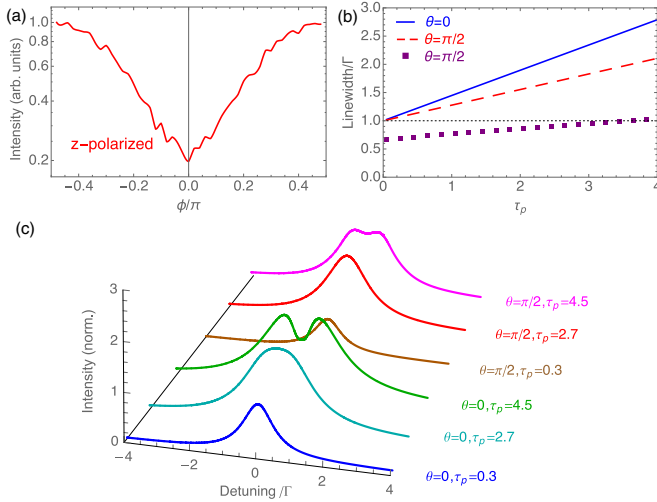


FIG. 8. RW model. (a) Distribution of on-resonance intensity in the plane  $\theta = \pi/2$ . Along the direction where single-scattering events are forbidden ( $\phi = 0$ ), the light intensity is suppressed. (b) The FWHM linewidth increases linearly with  $\tau_p$  in a dilute medium. The linewidth along the direction parallel to the laser polarization can drop below  $\Gamma$  for small  $\tau_p$  (purple squares). (c) Line shapes for different  $\tau_p$ 's and angles of observation. The line shape is Lorentzian for low  $\tau_p$  but gets distorted and develops a double-peak structure as the  $\tau_p$  increases. Here, for all angles, the signal is collected within a small angular region  $\delta\theta = 5^\circ$ . The intensity is normalized to the value at zero detuning for  $\theta = 0$  and  $\tau_p = 0.3$ , and the width of laser beam is 5 times the Gaussian width of the atomic cloud. Here, all  $\tau_p$  are labeled as the value at  $\Delta = 0$ .

The matrix  $\mathcal{R}(\phi)$  is the rotation matrix that rotates the incident axis  $\hat{e}_r$  to  $\hat{e}'_r$  (perpendicular to the scattering plane),

$$\mathcal{R}(\phi) = \begin{pmatrix} 1 & 0 & 0 & 0 \\ 0 & \cos(2\phi) & \sin(2\phi) & 0 \\ 0 & -\sin(2\phi) & \cos(2\phi) & 0 \\ 0 & 0 & 0 & 1 \end{pmatrix}, \quad (19)$$

and  $\mathcal{R}(\psi)$  is the rotation matrix that transforms the coordinate system  $\hat{e}'_1, \hat{e}'_2,$  and  $\hat{e}'_3$  back to the original coordinate system  $\hat{e}_1, \hat{e}_2,$  and  $\hat{e}_3$  and can be found from  $\theta$  and  $\phi$ . The polarization of the photons is encoded in the Stokes vector. The probability of a scattering event can be directly calculated from  $S''_0/S_0^{\text{in}}$ . Complete trajectories of the photons can be found from Monte Carlo sampling of scattering events. As the phase information of photon is not kept in this approach, it is more suitable for describing classical media or hot atoms where phase coherence is not important.

The polarization of the incident photon is randomized after multiple-scattering events. Since the intensity detected along the polarization direction of the incident photon requires at least two scattering events, it is suppressed compared to other directions but nonzero [Fig. 8(a)], and the linewidth at small  $\tau_p$  also drops below the natural linewidth [Fig. 8(c)] along this direction. For the other directions, the intensity distribution is roughly homogeneous and does not exhibit the collective enhancement along the forward direction observed in the coherent dipole model. The FWHM linewidth for different directions increases linearly with OD up to a moderate

value of OD [see Fig. 8(b)] and displays a polarization dependence similar to the prediction of CD. Under this classical treatment more scattering processes are expected to occur with increasing  $\tau_p$ , and those processes tend to inhibit the transmission of light. As the scattering becomes more frequent, forward scattering decreases, and more light is scattered backwards [44]. Since  $\tau_p$  is maximum at resonance,  $\Delta = 0$ , the linewidth develops a “double-peak” profile as the medium becomes denser [Fig. 8(c)]. Before the distortion in line shape develops, the FWHM linewidth also linearly increases with  $\tau_p$ . We note that a similar double-peak structure also appears in the coherent dipole model. However, there, it only happens at specific small angles [see Fig. 3(c)] and never happens along the forward direction, where the stimulated photon emission dominates, or the transverse direction, where the photons scattered via dipolar exchange dominate. We attribute the appearance of the double-peak structure to the interplay between these two types of emissions. In summary, despite the fact that the RW model does not include coherent emission mechanisms, it is able to reproduce the collective broadening observed with increasing optical depth and the subnatural linewidth present in the direction parallel to the laser polarization at relatively small optical depths. The RW model, on the other hand, ignores coherent elastic dipolar interactions and thus does not predict a density shift.

#### IV. ROLE OF ATOMIC MOTION

An assumption made in Sec. II is that the position of the atoms remains fixed. This assumption is valid only when atoms move at a rate slower than the radiative decay rate. When motion is significantly faster, e.g., hot atomic clouds, the coherence during radiation is smeared out, and classical approaches, such as the RW model, are usually satisfactory [40,42] to describe collective light emission. However, many experiments operate in an intermediate regime where coherences cannot be totally disregarded, and it is not a good approximation to treat atoms as frozen. For example, for the  $^1S_0 \rightarrow ^3P_1$  transition of  $^{88}\text{Sr}$  atoms, the Doppler broadening at  $\sim 1\mu\text{K}$ ,  $\Delta_D \approx 6\Gamma$ , and recoil frequency  $\omega_r = \hbar k_0^2/2m \approx 0.6\Gamma$ , both comparable to the natural linewidth [69,70]. Consequently, for a proper description of light scattering one needs to account for both photon coherences and atomic motion on an equal footing. Below we present two approximate ways to accomplish this.

##### A. Modified frozen dipole model

In this section, we discuss a simple way to include the effects of atomic motion on light scattering via a modified CD model. For a single atom, to leading order, a major modification from motion in the emitted light intensity is the Doppler shift, a velocity-dependent modification of the effective laser detuning experienced by an atom (see Appendix C). We include this effect in the many-body system by introducing random detunings for each atom, i.e.,  $\Delta \rightarrow \Delta + \delta\nu$ , and by sampling them according to a Maxwell-Boltzmann distribution  $P(\delta\nu) = \frac{1}{\sqrt{2\pi}\tilde{\Delta}_D} \exp(-\frac{\delta\nu^2}{2\tilde{\Delta}_D^2})$  that accounts for the Doppler shifts [22]. Here,  $\tilde{\Delta}_D = \Delta_D/\sqrt{8\ln 2}$ . We denote this approximation as the modified frozen dipole model. The random detunings modify atomic coherences as (for simplicity we assume a single beam

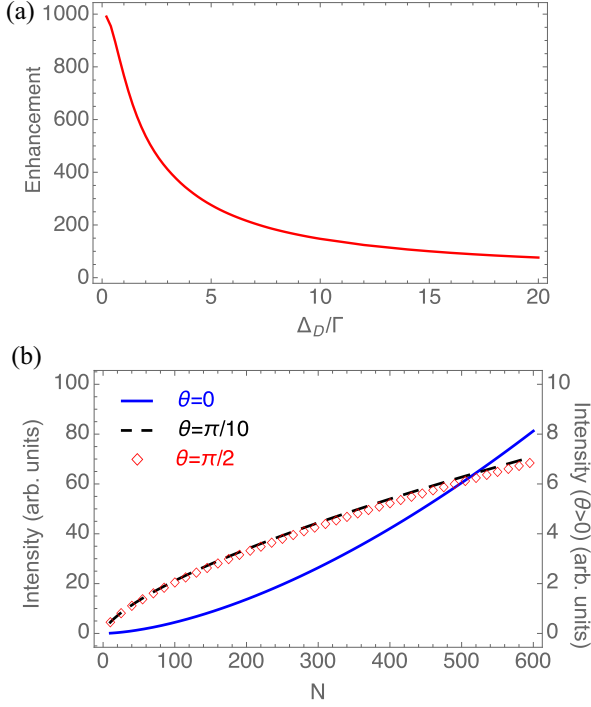


FIG. 9. Modified frozen dipole model: peak intensity. (a) Collective forward enhancement: forward intensity normalized by the transverse intensity as a function of Doppler width. (b) Intensity detected along different directions at Doppler width  $\Delta_D = 6\Gamma$  as a function of atom number for fixed cloud size (when  $N = 500$ ,  $\tau = 2$ ,  $n_0 k_0^{-3} = 0.0015$ ).  $I \sim N^{1.6}$  for  $\theta = 0$ , and  $I \sim N^{0.7}$  for  $\theta = \pi/2$ . The right vertical axis labels the intensity for  $\theta = \pi/2, \pi/10$ .

illumination)

$$b_j = \frac{\Omega e^{i\mathbf{k}_0 \cdot \mathbf{r}_j}}{(\Delta - \delta v_j) + i\Gamma/2}. \quad (20)$$

Using Eq. (20), the intensity along a generic direction becomes

$$I_{\text{incoh}} = \frac{1}{\sqrt{2\pi} \tilde{\Delta}_D} \int d\delta v_j |b_j|^2 e^{-\delta v_j^2 / 2\tilde{\Delta}_D^2}. \quad (21)$$

On the other hand, the coherent scattering in the forward direction which takes into account pairwise atomic contributions becomes

$$I_{\text{coh}} = \frac{1}{2\pi \tilde{\Delta}_D^2} \int d\delta v_j d\delta v_{j'} b_j b_{j'}^* e^{-\delta v_j^2 / 2\tilde{\Delta}_D^2} e^{-\delta v_{j'}^2 / 2\tilde{\Delta}_D^2}. \quad (22)$$

The on-resonance enhancement factor is thus

$$\frac{I_{\text{coh}}}{I_{\text{incoh}}} = \frac{\sqrt{\frac{\pi}{2}} e^{\frac{8\tilde{\Delta}_D^2}{\Gamma^2}} \text{erfc}\left(\frac{1}{2\sqrt{2}\tilde{\Delta}_D/\Gamma}\right)}{2\tilde{\Delta}_D/\Gamma}, \quad (23)$$

where  $\text{erfc}$  is the complementary error function. This induces an exponential suppression of the forward interference that depends on  $\tilde{\Delta}_D/\Gamma$  [53], as shown in Fig. 9(a).

The reduced light scattering probability, on the other hand, competes with dephasing since it suppresses multiple scattering and, as a consequence, promotes collective enhancement. Effectively, it brings the system closer to the small-OD regime [Fig. 2(b)]. The motion-induced suppression of multiscattering processes is also signaled in the frequency shift (Fig. 4)

[22,27], which keeps increasing until a larger value of density in the presence of motion.

## B. Semiclassical approach

Laser-light-mediated forces on atoms are a fundamental concept in atomic physics and lay the foundations of laser trapping and cooling [64,71]. They can be accounted for at the semiclassical level by explicitly including the position  $\mathbf{r}_i$  and the momentum  $\mathbf{p}_i$  degrees of freedom of the atoms and solving for their dynamics while feeding those back into the quantum dynamics of the internal degrees of freedom. An explicit description of this procedure is presented below.

For simplicity we will assume a two-level transition. This condition is achievable in experiments, for example, by applying a large magnetic field to split apart ( $|\Delta^\alpha - \Delta^\gamma| \gg \mathcal{G}\Gamma$ ) the excited-state levels and thus energetically suppressing the population of the ones not directly driven by the laser. For driving the atoms we will consider the case of two counterpropagating lasers with wave vector  $\pm\mathbf{k}_0$ , propagating along  $x$ , and Rabi frequency  $\Omega$ . The internal atomic variables evolve according to (see Appendix A)

$$\begin{aligned} \frac{db_j}{dt} = & i\Omega \cos(\mathbf{k}_0 \cdot \mathbf{r}_j) s_j - \left(\frac{\Gamma}{2} + i\Delta\right) b_j \\ & + i \sum_{l \neq j} s_j b_l (g_{jl} - i f_{jl}), \end{aligned} \quad (24)$$

$$\begin{aligned} \frac{ds_j}{dt} = & 2i\Omega \cos(\mathbf{k}_0 \cdot \mathbf{r}_j) (b_j - \text{H.c.}) - \Gamma s_j \\ & - 2i \sum_{l \neq j} (g_{jl} - i f_{jl}) b_j^* b_l + 2i \sum_{l \neq j} (g_{jl} + i f_{jl}) b_l^* b_j, \end{aligned} \quad (25)$$

where  $\Delta = \Delta^\alpha$  and the last terms describe the effect of dipole-dipole interactions  $g(r)$  and  $f(r)$  (see Appendix A). In general the position of atoms can also change with time as

$$\frac{d\mathbf{r}_j}{dt} = \frac{\mathbf{p}_j}{m}, \quad (26)$$

so the response to the local driving field and dipole-dipole interactions in Eqs. (24) and (25) change accordingly. The momentum changes due to not only the force exerted by the driving laser but also the long-range forces  $g_{jl} = -\nabla g_{jl}$  and  $f_{jl} = -\nabla f_{jl}$ , which originate from the dispersive and dissipative dipole-dipole interactions, respectively (see Appendix A), and depend on the instantaneous atomic coherences and positions:

$$\begin{aligned} \frac{d\mathbf{p}_j}{dt} = & -2\hbar\mathbf{k}_0\Omega \sin(\mathbf{k}_0 \cdot \mathbf{r}_j) \text{Re}\{b_j(t)\} \\ & + \sum_{l \neq j} [g_{jl}(b_j b_l^* + \text{H.c.}) - i f_{jl}(b_j b_l^* - \text{H.c.})]. \end{aligned} \quad (27)$$

The atomic coherence and external motion are now coupled together, so Eqs. (24)–(27) need to be solved simultaneously to obtain the dynamics. In deriving Eq. (27), we have ignored the role of momentum diffusion (see Appendix A). We have verified in our numerical simulations that it can be safely ignored for the parameters of interest presented in this work.

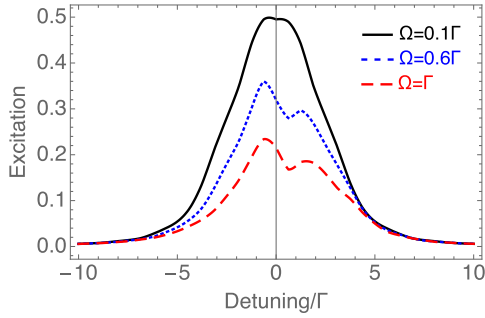


FIG. 10. Semiclassical model: single-atom line shape. The excitation line shape is calculated for three different driving strengths, each normalized by  $\Omega^2$ . The atomic motion is allowed to be one-dimensional and parallel to the laser propagating direction. Here, we used  $\omega_r = 0.6\Gamma$  (the value of the  $^1S_0 \rightarrow ^3P_1$  transition of Sr [69]).

In previous sections, it has been shown that except for a narrow cone around the forward direction, the fluorescence intensity is  $I(\mathbf{r}_s) \propto \sum_i s_i$  (also see Appendix C). Since we expect motion to further reduce the effect of coherence, we will focus on the transverse scattering and compute  $\sum_i s_i$ . Figure 10 shows the line shape of a single atom for different  $\Omega$  calculated from the semiclassical approach.

As a result of atomic motion, the laser-atom system is not in a stationary state. We show the results for driving time  $t = 5/\Gamma$ . When  $\Omega \ll \Gamma$ , the line shape is a Voigt profile with the Doppler width determined by the velocity. When  $\Omega \sim \Gamma$ , there is a distortion in the line shape, with more intensity at  $\Delta < 0$ . This is because for  $\Delta < 0$  the laser force decelerates the atom, while for  $\Delta > 0$  the atom is heated up. With reduced (increased) velocity, the atom is, on average, more (less) excited, resulting in a distorted line shape. The center of the line is therefore shifted to the red.

Motion can significantly modify the interactions between atoms [72]. We study the effect of motion on the frequency shift in Fig. 11. Dipolar-induced frequency shifts were previously discussed in Sec. II. Since we focus on low driving fields, again we neglect momentum diffusion in these calculations. The calculations show that unless  $\Delta_D$  is very small, atomic

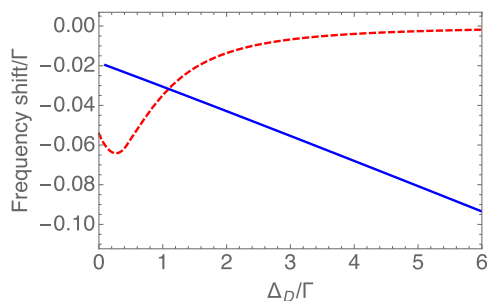


FIG. 11. Semiclassical model: effect of motion on frequency shift. Two atoms are driven by a pair of counterpropagating lasers, with  $\Omega = 0.1\Gamma$ ,  $\omega_r = 0.6\Gamma$ . The red dashed line shows the result of the semiclassical model where motion is allowed in three dimensions. The blue solid line shows the result from the modified CD. The center of the excitation line shape is calculated at  $t = 5/\Gamma$  for different Doppler widths for both models.

motion leads to a fast suppression of the frequency shift. Only when  $\Delta_D \ll \Gamma$  can the frequency be increased by motion, and this is the regime where the modified frozen dipole model is qualitatively valid; recall that it predicts always an increase of density shift with Doppler broadening. We note that at  $\Delta_D \rightarrow 0$  the frequency shift obtained using the modified frozen dipole model is slightly smaller than that obtained from the semiclassical approach. This is a consequence of the distortion caused by laser cooling or heating, which additionally shifts the spectral line. For  $\Delta_D \gtrsim \Gamma$  motion needs to be properly accounted for, and the modified frozen dipole model is not reliable.

## V. CONCLUSION

We theoretically studied the propagation of light through a cold atomic medium. We presented two different microscopic models, the coherent dipole model and the random-walk model, and analyzed how the light polarization, optical depth, and density affect the linewidth broadening, intensity, and line-center shift of the emitted light. We showed that the random-walk model, which neglects photonic phase coherence, can fairly capture the collective broadening (narrowing) of the emission linewidth but, on the other hand, does not predict a density shift. Due to the limitation of computation capacity, the numerical simulation of CD is usually restricted to  $\sim 10^4$  atoms, which is much smaller than that in some cold-atom experiments [9,62]. Nevertheless, the understanding of the underlying physics allowed us to perform an appropriate rescaling in the cloud size which we used to compare with experiments [53]. We further developed generalized models that explicitly take into account motional effects. We showed that atomic motion can lead to drastic dephasing and reduction in the collective effects, together with a distortion in the line shape. While the modified frozen dipole model predicts a monotonic increase of the density shift with increasing motion, the semiclassical model, which properly accounts for recoil effects, predicts that this behavior holds only at slow motion  $\Delta_D \ll \Gamma$ . Instead, as atoms move faster, motional effects start to become dominant, the cloud expands, and the frequency shift decreases. None of the presented theoretical models, however, can explain the large density shift measured in the  $^1S_0 \rightarrow ^3P_1$  transition of  $^{88}\text{Sr}$  atoms [69]. It will be intriguing to determine what the actual physical processes are that cause this large shift.

## ACKNOWLEDGMENTS

The authors wish to acknowledge useful discussions with the JILA Ye group, A. Gorshkov, J. Javanainen, M. Havey, M. Holland, M. L. Wall, J. D’Incao, M. Davis, and J. Schachenmayer. We would like to especially thank R. Kaiser for helpful discussions and insightful comments. This work was supported by the NSF (Grants No. PHY-1211914, No. PHY-1521080, and No. PFC-PHY-1125844), AFOSR (Grant No. FA9550-13-1-0086), AFOSR MURI ADVANCED QUANTUM MATERIALS, and ARO (Grant No. W911NF-12-1-0228). Computations utilized the Janus supercomputer, supported by the National Science Foundation (Award No. CNS-0821794) and the University of Colorado Boulder.

### APPENDIX A: LONG-RANGE DIPOLE-DIPOLE INTERACTION, FORCE, AND DIFFUSION

Here, we derive the form of dipole-dipole interactions and the corresponding forces for two-level moving atoms, with  $\omega_a = k_0 c$  being the frequency of transition and  $\mathbf{d}$  being the dipole moment. We include motion in the dipolar coupling after eliminating the electromagnetic vacuum modes. The Hamiltonian, including the atoms and free-space electromagnetic field, is

$$H = \hbar\omega_a \sum_j \hat{b}_j^\dagger \hat{b}_j + \sum_{\mathbf{k}, \epsilon} \omega_k \hat{a}_{\mathbf{k}\epsilon}^\dagger \hat{a}_{\mathbf{k}\epsilon} - \sum_j \sum_{\mathbf{k}, \epsilon} g_k \times (\mathbf{d} \cdot \hat{\epsilon}_{\mathbf{k}}) [(e^{i\mathbf{k}\cdot\mathbf{r}_j} \hat{a}_{\mathbf{k}\epsilon} + \text{H.c.}) (\hat{b}_j^\dagger + \text{H.c.})]. \quad (\text{A1})$$

The atomic dipoles and field modes evolve according to

$$\frac{d\hat{a}_{\mathbf{k}\epsilon}}{dt} = -i\omega_k \hat{a}_{\mathbf{k}\epsilon} + \frac{i}{\hbar} \sum_j g_k (\mathbf{d}_j \cdot \hat{\epsilon}_{\mathbf{k}}) [e^{-i\mathbf{k}\cdot\mathbf{r}_j} (\hat{b}_j + \text{H.c.})], \quad (\text{A2})$$

$$\frac{d\hat{b}_j}{dt} = -i\omega_a \hat{b}_j + i \sum_{\mathbf{k}, \epsilon} \frac{g_k}{\hbar} (\mathbf{d}_j \cdot \hat{\epsilon}_{\mathbf{k}}) [e^{i\mathbf{k}\cdot\mathbf{r}_j} \hat{a}_{\mathbf{k}\epsilon} \hat{s}_j + \text{H.c.}], \quad (\text{A3})$$

$$\frac{d\hat{s}_j}{dt} = -i \sum_{\mathbf{k}, \epsilon} \frac{g_k}{\hbar} (\mathbf{d}_j \cdot \hat{\epsilon}_{\mathbf{k}}) [e^{i\mathbf{k}\cdot\mathbf{r}_j} \hat{a}_{\mathbf{k}\epsilon} \hat{b}_j^\dagger - e^{-i\mathbf{k}\cdot\mathbf{r}_j} \hat{a}_{\mathbf{k}\epsilon}^\dagger \hat{b}_j - e^{i\mathbf{k}\cdot\mathbf{r}_j} \hat{a}_{\mathbf{k}\epsilon} \hat{b}_j + e^{-i\mathbf{k}\cdot\mathbf{r}_j} \hat{a}_{\mathbf{k}\epsilon}^\dagger \hat{b}_j^\dagger], \quad (\text{A4})$$

where  $\hat{s}_j = \hat{b}_j^\dagger \hat{b}_j - \hat{b}_j \hat{b}_j^\dagger$  and  $s_j = \langle \hat{s}_j \rangle$  gives the inversion of the  $j$ th atom. We have assumed that internal operators commute with external operators and neglected the diffusion of the atomic wave packet. Equation (A2) can be formally integrated to obtain

$$\hat{a}_{\mathbf{k}\epsilon}(t) = \hat{a}_{\mathbf{k}\epsilon}(0) - i \sum_j \frac{g_k}{\hbar} (\mathbf{d}_j \cdot \hat{\epsilon}_{\mathbf{k}}) \int dt' e^{i\mathbf{k}\cdot\mathbf{r}_j + i\omega_k(t'-t)} \times (\hat{b}_j + \text{H.c.}). \quad (\text{A5})$$

Assuming the external motion is much slower than the internal dynamics relevant inside the integral, so that  $\mathbf{r}_j(t') \approx \mathbf{r}_j(t)$ , and the interaction between atoms and the field modes is weak so that  $\hat{b}_j(t') \approx \hat{b}_j(t) e^{-i\omega_a(t'-t)}$ , and substituting Eq. (A5) into Eq. (A3), we obtain the equation for the quantum averaged quantities:

$$\begin{aligned} \frac{d\hat{b}_j}{dt} = & -i\omega_a \hat{b}_j + \hat{s}_j \sum_l \sum_{\mathbf{k}, \epsilon} \frac{g_k^2}{\hbar^2} (\mathbf{d}_j \cdot \hat{\epsilon}_{\mathbf{k}}) (\mathbf{d}_l \cdot \hat{\epsilon}_{\mathbf{k}}) \\ & \times \left\{ e^{i\mathbf{k}\cdot\mathbf{r}_{jl}} \left[ \hat{b}_l^\dagger \left( \pi \delta(\omega_k + \omega_a) - iP \frac{1}{\omega_k + \omega_a} \right) \right. \right. \\ & \left. \left. + \hat{b}_l \left( \pi \delta(\omega_k - \omega_a) - iP \frac{1}{\omega_k - \omega_a} \right) \right] \right. \\ & \left. - e^{-i\mathbf{k}\cdot\mathbf{r}_{jl}} \left[ \hat{b}_l^\dagger \left( \pi \delta(\omega_k - \omega_a) + iP \frac{1}{\omega_k - \omega_a} \right) \right. \right. \\ & \left. \left. + \hat{b}_l \left( \pi \delta(\omega_k + \omega_a) + iP \frac{1}{\omega_k + \omega_a} \right) \right] \right\}, \quad (\text{A6}) \end{aligned}$$

where we have utilized the fact that  $\langle \hat{a}_{\mathbf{k}\epsilon}(0) \rangle = 0$  and assumed that atomic motion is classical [73,74]. Changing  $\sum_{\mathbf{k}} = \frac{V}{(2\pi)^3} \int d\Omega dk k^2$  and applying a rotating-wave approximation, we have

$$\frac{d\hat{b}_j}{dt} = -i\omega_a \hat{b}_j + i \sum_{l \neq j} \hat{s}_j \hat{b}_l (g_{jl} - i f_{jl}) - \frac{\Gamma}{2} \hat{b}_j, \quad (\text{A7})$$

with  $f(0) = \Gamma$ , and

$$g(r) = -\frac{3\Gamma}{4} \left[ z_1(\theta) \frac{\cos k_0 r}{k_0 r} + z_2(\theta) \left( \frac{\cos k_0 r}{k_0^3 r^3} + \frac{\sin k_0 r}{k_0^2 r^2} \right) \right], \quad (\text{A8})$$

$$f(r) = \frac{3\Gamma}{4} \left[ z_1(\theta) \frac{\sin k_0 r}{k_0 r} + z_2(\theta) \left( \frac{\sin k_0 r}{k_0^3 r^3} - \frac{\cos k_0 r}{k_0^2 r^2} \right) \right], \quad (\text{A9})$$

where  $z_1(\theta) = \sin^2 \theta$  and  $z_2(\theta) = (3\cos^2 \theta - 1)$ . These expressions can also be obtained from Eqs. (5)–(9) by keeping only a single  $\alpha$  component. We further assume that multiatom correlations can be factorized,  $\langle \hat{s}_j \hat{b}_l \rangle \approx \langle \hat{s}_j \rangle \langle \hat{b}_l \rangle$ , so that the atomic coherence evolves as

$$\frac{db_j}{dt} = -i\omega_a b_j + i \sum_{l \neq j} s_j b_l (g_{jl} - i f_{jl}) - \frac{\Gamma}{2} b_j, \quad (\text{A10})$$

where  $\mathcal{O} = \langle \hat{\mathcal{O}} \rangle$  for any atomic operator  $\hat{\mathcal{O}}$ . It is coupled to  $s_j$ , the equation of which can be derived in a similar way and is given by

$$\begin{aligned} \frac{ds_j}{dt} = & -\Gamma s_j - 2i \sum_{l \neq j} (g_{jl} - i f_{jl}) b_j^* b_l \\ & + 2i \sum_{l \neq j} (g_{jl} + i f_{jl}) b_l^* b_j. \quad (\text{A11}) \end{aligned}$$

If we consider very low external driving field and  $s_j \approx -1$ , Eq. (A10) is decoupled from  $s_j$  and can be reduced to the form of Eq. (10). For the momentum,

$$\begin{aligned} \frac{d\hat{\mathbf{p}}_j}{dt} = & -\nabla \hat{H} \\ = & - \sum_{\mathbf{k}, \epsilon} g_k (\mathbf{d}_j \cdot \hat{\epsilon}_{\mathbf{k}}) (i\mathbf{k} e^{i\mathbf{k}\cdot\mathbf{r}_j} \hat{a}_{\mathbf{k}\epsilon} \hat{b}_j^\dagger - i\mathbf{k} e^{-i\mathbf{k}\cdot\mathbf{r}_j} \hat{a}_{\mathbf{k}\epsilon}^\dagger \hat{b}_j \\ & + i\mathbf{k} e^{i\mathbf{k}\cdot\mathbf{r}_j} \hat{a}_{\mathbf{k}\epsilon} \hat{b}_j - i\mathbf{k} e^{-i\mathbf{k}\cdot\mathbf{r}_j} \hat{a}_{\mathbf{k}\epsilon}^\dagger \hat{b}_j^\dagger). \quad (\text{A12}) \end{aligned}$$

After substituting Eq. (A5), taking the quantum average, and performing an integration procedure similar to that above, we obtain

$$\frac{d\mathbf{p}_j}{dt} = \sum_{l \neq j} [g_{jl} (b_j b_l^* + \text{H.c.}) - i f_{jl} (b_j b_l^* - \text{H.c.})], \quad (\text{A13})$$

with  $g_{jl} = -\nabla g_{jl}$  and  $f_{jl} = -\nabla f_{jl}$ . As the dispersive force  $g_{jl}$  is a steep function of  $r_{jl}$ , it dominates at short distances, and atoms are drastically accelerated or decelerated. Both the dispersive and dissipative forces are anisotropic and couple motion along different directions.

Due to the presence of spontaneous emission and radiative interactions, the atomic momentum also diffuses over time, which can be described by including classical noise  $d\xi_i^\alpha$  in the

equation of motion for  $p_i^\alpha$ . The components of these noises are correlated and are characterized by the diffusion matrix

$$E[d\xi_i^\alpha(t)d\xi_i^\beta(t')] = \delta_{\alpha,\beta} \frac{2 - \delta_{\alpha,z}}{10} \hbar^2 k_0^2 \Gamma (s_i + 1) \delta(t - t'), \quad (\text{A14})$$

$$E[d\xi_i^\alpha(t)d\xi_j^\beta(t')] = -2\hbar^2 k_0^2 \nabla_\alpha \nabla_\beta f(r_{ij}) \text{Re}[b_i^* b_j] \delta(t - t'), \quad (\text{A15})$$

where  $E[\cdot]$  denotes the expectation value.

The momentum diffusion matrix can be found from

$$\begin{aligned} \mathcal{D}_{jl} &= \frac{d\langle \hat{\mathbf{p}}_j \hat{\mathbf{p}}_l \rangle}{dt} - \langle \mathbf{p}_j \rangle \frac{d\langle \mathbf{p}_l \rangle}{dt} - \frac{d\langle \mathbf{p}_j \rangle}{dt} \langle \mathbf{p}_l \rangle \quad (\text{A16}) \\ &= \sum_{\mathbf{k}_1, \epsilon_1} \sum_{\mathbf{k}_2, \epsilon_2} g_{k_1} g_{k_2} (\mathbf{d}_j \cdot \epsilon_1) (\mathbf{d}_l \cdot \epsilon_2) (i\mathbf{k}_1 e^{i\mathbf{k}_1 \cdot \mathbf{r}_j} \hat{a}_{\mathbf{k}_1 \epsilon_1}^\dagger \hat{b}_j^\dagger \\ &\quad - i\mathbf{k}_1 e^{-i\mathbf{k}_1 \cdot \mathbf{r}_j} \hat{a}_{\mathbf{k}_1 \epsilon_1}^\dagger \hat{b}_j) \\ &\quad + i\mathbf{k}_1 e^{i\mathbf{k}_1 \cdot \mathbf{r}_j} \hat{a}_{\mathbf{k}_1 \epsilon_1} \hat{b}_j - i\mathbf{k}_1 e^{-i\mathbf{k}_1 \cdot \mathbf{r}_j} \hat{a}_{\mathbf{k}_1 \epsilon_1} \hat{b}_j^\dagger \\ &\quad \times (i\mathbf{k}_2 e^{i\mathbf{k}_2 \cdot \mathbf{r}_l} \hat{a}_{\mathbf{k}_2 \epsilon_2}^\dagger \hat{b}_l^\dagger - i\mathbf{k}_2 e^{-i\mathbf{k}_2 \cdot \mathbf{r}_l} \hat{a}_{\mathbf{k}_2 \epsilon_2}^\dagger \hat{b}_l) \\ &\quad + i\mathbf{k}_2 e^{i\mathbf{k}_2 \cdot \mathbf{r}_l} \hat{a}_{\mathbf{k}_2 \epsilon_2} \hat{b}_l - i\mathbf{k}_2 e^{-i\mathbf{k}_2 \cdot \mathbf{r}_l} \hat{a}_{\mathbf{k}_2 \epsilon_2} \hat{b}_l^\dagger) \\ &= -2\hbar^2 k_0^2 \nabla \nabla f_{ij} \text{Re}[b_j^* b_l]. \end{aligned} \quad (\text{A17})$$

In dense clouds momentum diffusion from radiative interactions can give rise at long times to significant heating. This heating was reported to be one of the main limiting mechanisms in laser cooling [74,75]. At short times,  $t\Gamma \sim 1$ , with low densities and weak probes,  $\Omega < \Gamma$ , the momentum diffusion is not prominent, and since this is the regime we are interested in this work, we ignore momentum diffusion in our calculations presented in the main text.

## APPENDIX B: OPTICAL DEPTH OF A CLOUD WITH GAUSSIAN DISTRIBUTION

We consider an atomic cloud with a Gaussian distribution  $n(x, y, z) = n_0 e^{-\frac{x^2}{2R_x^2} - \frac{y^2}{2R_y^2} - \frac{z^2}{2R_z^2}}$ , where  $n_0$  satisfies  $\int dx dy dz n(x, y, z) = N$  and  $N$  is the total number of atoms. Along the line of observation, e.g.,  $\hat{x}$ , the on-resonance optical depth is related to the resonant scattering cross section, which for the  $J = 0 \rightarrow J' = 1$  transition is  $\sigma_{sc} = \sigma_0(\Delta = 0) = \frac{6\pi}{k_0^2}$ , and the column density averaged over the profile perpendicular to this direction [19,47],

$$\begin{aligned} \tau &= \left[ \int dy dz n(y, z) \right]^{-1} \int dy dz n(y, z) \tau(y, z) \\ &= \left[ \int dy dz n(y, z) \right]^{-1} \int dy dz n(y, z) \int dx n(x, y, z) \sigma_{sc} \\ &= \left[ \int dy dz n(y, z) \right]^{-1} \int dy dz n(y, z) e^{-\frac{y^2}{2R_y^2} - \frac{z^2}{2R_z^2}} \\ &\quad \times \int dx n_0 e^{-\frac{x^2}{2R_x^2}} \sigma_{sc} \end{aligned}$$

$$\begin{aligned} &= \frac{3N}{2k_0^2 R_y R_z} \\ &= \frac{3N}{2k_0^2 R_\perp^2}. \end{aligned} \quad (\text{B1})$$

With laser detuning  $\Delta$ , the optical depth is  $\tau/(1 + 4\Delta^2/\Gamma^2)$ .

## APPENDIX C: EFFECT OF MOTION ON SINGLE-ATOM FLUORESCENCE

Here, we derive the fluorescence intensity emitted by a weakly driven atom, using a full quantum approach with the motional effect included. We consider the states including at most one excitation, and label the relevant quantum states by  $|\mathbf{p}\alpha, 0\rangle, |\mathbf{p}g, \mathbf{k}_\epsilon\rangle$ , with  $\alpha = \{e, g\}$ ,  $\mathbf{p}$  being the momentum of the atom, and  $\mathbf{k}(\epsilon)$  being the momentum (polarization) of the photon in vacuum ( $|\mathbf{p}\alpha, 0\rangle$  stands for no photon). For generality we assume here that two counterpropagating lasers are used to drive the atoms, carrying momenta  $\mathbf{k}_0$  and  $-\mathbf{k}_0$ , respectively. The Hamiltonian is [76]

$$\begin{aligned} \hat{H} &= \frac{\hat{\mathbf{p}}^2}{2m} + \hbar\omega_a \hat{b}^\dagger \hat{b} + \hbar\Omega [\cos(\mathbf{k}_0 \cdot \mathbf{r}) (e^{-i\omega_L t} \hat{b}^\dagger + \text{H.c.})] \\ &\quad + \sum_{\mathbf{k}, \epsilon} \hbar\omega_k \hat{a}_{\mathbf{k}\epsilon}^\dagger \hat{a}_{\mathbf{k}\epsilon} - \hbar \sum_{\mathbf{k}, \epsilon} (\mathbf{d} \cdot \hat{\epsilon}_{\mathbf{k}}) g_k [e^{i\mathbf{k} \cdot \mathbf{r}} \hat{a}_{\mathbf{k}\epsilon} \hat{b}^\dagger + \text{H.c.}]. \end{aligned} \quad (\text{C1})$$

The state vector of the system is

$$\begin{aligned} |\psi\rangle &= \sum_\alpha \int d\mathbf{p} |\mathbf{p}\alpha, 0\rangle A_{\alpha 0}(\mathbf{p}, t) e^{-i(E_\alpha + E_p)t/\hbar} \\ &\quad + \sum_{\mathbf{k}, \epsilon} \int d\mathbf{p} |\mathbf{p}g, \mathbf{k}_\epsilon\rangle B_{g\mathbf{k}\epsilon}(\mathbf{p}, t) e^{-i(E_g + E_p + \hbar\omega_k)t/\hbar}, \end{aligned} \quad (\text{C2})$$

where  $E_\alpha = \omega_\alpha \delta_{\alpha, e}$ ,  $E_p = \frac{p^2}{2m}$ ,  $|A_{\alpha 0}(\mathbf{p}, t)|^2$  represents the population in the state  $\alpha$  possessing momentum  $\mathbf{p}$ , and  $B_{g\mathbf{k}\epsilon}(\mathbf{p}, t)$  is the amplitude of having a photon  $\mathbf{k}$  with polarization  $\epsilon$ . The state of the system evolves according to

$$\begin{aligned} i \frac{dA_{g0}(\mathbf{p}, t)}{dt} &= \Omega A_{e0}(\mathbf{p} + \mathbf{k}, t) e^{i(\omega_L - \omega_a)t} e^{-iE_{\mathbf{p}+\mathbf{k}, \mathbf{p}}t/\hbar} \\ &\quad + \Omega A_{e0}(\mathbf{p} - \mathbf{k}, t) e^{i(\omega_L - \omega_a)t} e^{-iE_{\mathbf{p}-\mathbf{k}, \mathbf{p}}t/\hbar}, \end{aligned} \quad (\text{C3})$$

$$\begin{aligned} i \frac{dA_{e0}(\mathbf{p}, t)}{dt} &= - \sum_{\mathbf{k}, \epsilon} (\mathbf{d} \cdot \hat{\epsilon}_{\mathbf{k}}) g_k B_{g\mathbf{k}\epsilon}(\mathbf{p} - \mathbf{k}, t) \\ &\quad \times e^{-i(\omega_k - \omega_a)t} e^{-iE_{\mathbf{p}-\mathbf{k}, \mathbf{p}}t/\hbar} \\ &\quad + \Omega A_{g0}(\mathbf{p} - \mathbf{k}, t) e^{-i(\omega_L - \omega_a)t} e^{-iE_{\mathbf{p}-\mathbf{k}, \mathbf{p}}t/\hbar} \\ &\quad + \Omega A_{g0}(\mathbf{p} + \mathbf{k}, t) e^{-i(\omega_L - \omega_a)t} e^{-iE_{\mathbf{p}+\mathbf{k}, \mathbf{p}}t/\hbar}, \end{aligned} \quad (\text{C4})$$

$$i \frac{dB_{gk\epsilon}(\mathbf{p}, t)}{dt} = B_{gk\epsilon}(\mathbf{p}, t) - (\mathbf{d} \cdot \hat{\mathbf{e}}_{\mathbf{k}}) g_k A_{e0}(\mathbf{p} + \mathbf{k}, t) \times e^{i(\omega_k - \omega_a)t} e^{-iE_{\mathbf{p}+\mathbf{k}, p}t/\hbar}, \quad (\text{C5})$$

where  $E_{p_1, p_2} = \frac{p_1^2 - p_2^2}{2m}$ . The first term in Eq. (C4) describes the effect of vacuum photons, which, according to the Wigner-Weisskopf approach, leads to the spontaneous decay with rate  $\Gamma$  and can be rewritten as [77]

$$i \frac{dA_{e0}(\mathbf{p}, t)}{dt} = -i \frac{\Gamma}{2} A_{e0}(\mathbf{p}, t) + \Omega A_{g0}(\mathbf{p} - \mathbf{k}, t) \times e^{-i(\omega_L - \omega_a)t} e^{-iE_{\mathbf{p}-\mathbf{k}_0, p}t/\hbar} + \Omega A_{g0}(\mathbf{p} + \mathbf{k}, t) e^{-i(\omega_L - \omega_a)t} e^{-iE_{\mathbf{p}+\mathbf{k}_0, p}t/\hbar}. \quad (\text{C6})$$

Consider the initial condition  $B_{gk\epsilon}(\mathbf{p}, 0) = 0$ ,  $A_{g0} = \delta(\mathbf{p} - \mathbf{p}_0)$ , where  $\mathbf{p}_0$  is the initial momentum of the atom. The steady-state solution is

$$A_{e0}(\mathbf{p}, \infty) = \frac{\Omega[\delta(\mathbf{p}_0 - \mathbf{p} + \mathbf{k}_0) + \delta(\mathbf{p}_0 - \mathbf{p} - \mathbf{k}_0)]}{\Delta_L + E_{\mathbf{p}_0, \mathbf{p}} + i \frac{\Gamma}{2}}, \quad (\text{C7})$$

with  $\Delta_L = \omega_L - \omega_a$ . Thus, the atomic excitation  $\mathcal{A}_e = \int d\mathbf{p} |A_{e0}(\mathbf{p}, \infty)|^2$  indicates two Lorentzians with FWHM

equal to  $\Gamma$  and centered at  $\omega_r \pm \frac{\mathbf{k}_0 \cdot \mathbf{p}_0}{m}$ . The photon emission rate along a given direction  $\mathbf{k}_s$  is

$$I_{\mathbf{k}_s} = \frac{V\hbar c}{(2\pi)^3} \int dk k^3 \sum_{\epsilon} \int d\mathbf{p} \lim_{t \rightarrow \infty} \frac{|B_{gk\epsilon}(\mathbf{p}, t)|^2}{t}, \quad (\text{C8})$$

with  $\mathbf{k} = k\hat{\mathbf{k}}_s$ . We consider the transverse intensity case, where  $\mathbf{k} \cdot \mathbf{k}_0 = 0$ , and for atomic transitions  $\omega_r, \mathbf{p}_0 \cdot \mathbf{k}_0/m \ll \omega_L$ ; then

$$I_{\mathbf{k}_s} \approx \frac{\omega_L^4}{c^3} \frac{d^2 \Omega^2}{8\pi^2 \epsilon_0} \left[ \frac{1}{(\Delta - \omega_r + \frac{\mathbf{k}_0 \cdot \mathbf{p}_0}{m})^2 + \frac{\Gamma^2}{4}} + \frac{1}{(\Delta - \omega_r - \frac{\mathbf{k}_0 \cdot \mathbf{p}_0}{m})^2 + \frac{\Gamma^2}{4}} \right]. \quad (\text{C9})$$

The emitted light intensity exhibits the same profile as the atomic excitation  $\mathcal{A}_e$ .

As indicated by the above expression, motion modifies the emitted light intensity by adding two natural corrections: a Doppler shift  $\propto \frac{\mathbf{k}_0 \cdot \mathbf{p}_0}{m}$ , modifying the effective laser detuning, and a velocity-independent recoil shift  $\omega_r$ , which physically accounts for the fact that to compensate for the energy imparted to the atom via photon recoil, the incident laser needs to have a higher frequency to be resonant with the atomic transition.

- 
- [1] H. J. Kimble, *Nature (London)* **453**, 1023 (2008).  
[2] J. I. Cirac, P. Zoller, H. J. Kimble, and H. Mabuchi, *Phys. Rev. Lett.* **78**, 3221 (1997).  
[3] H. De Riedmatten, M. Afzelius, M. U. Staudt, C. Simon, and N. Gisin, *Nature (London)* **456**, 773 (2008).  
[4] J. S. Douglas, H. Habibian, C.-L. Hung, A. Gorshkov, H. J. Kimble, and D. E. Chang, *Nat. Photonics* **9**, 326 (2015).  
[5] I. Bloch, *Nat. Phys.* **1**, 23 (2005).  
[6] G. Jotzu, M. Messer, R. Desbuquois, M. Lebrat, T. Uehlinger, D. Greif, and T. Esslinger, *Nature (London)* **515**, 237 (2014).  
[7] I. Bloch, J. Dalibard, and S. Nascimbène, *Nat. Phys.* **8**, 267 (2012).  
[8] J. G. Bohnet, Z. Chen, J. M. Weiner, D. Meiser, M. J. Holland, and J. K. Thompson, *Nature (London)* **484**, 78 (2012).  
[9] W. Guerin, M. O. Araújo, and R. Kaiser, *Phys. Rev. Lett.* **116**, 083601 (2016).  
[10] A. H. Safavi-Naeini, T. M. Alegre, J. Chan, M. Eichenfield, M. Winger, Q. Lin, J. T. Hill, D. Chang, and O. Painter, *Nature (London)* **472**, 69 (2011).  
[11] A. Ourjoumtsev, A. Kubanek, M. Koch, C. Sames, P. W. Pinkse, G. Rempe, and K. Murr, *Nature (London)* **474**, 623 (2011).  
[12] D. W. Brooks, T. Botter, S. Schreppler, T. P. Purdy, N. Brahms, and D. M. Stamper-Kurn, *Nature (London)* **488**, 476 (2012).  
[13] D. F. V. James, *Phys. Rev. A* **47**, 1336 (1993).  
[14] R. H. Lehmburg, *Phys. Rev. A* **2**, 883 (1970).  
[15] J. Ruostekoski and J. Javanainen, *Phys. Rev. A* **55**, 513 (1997).  
[16] J. Javanainen, J. Ruostekoski, B. Vestergaard, and M. R. Francis, *Phys. Rev. A* **59**, 649 (1999).  
[17] M. O. Scully, E. S. Fry, C. H. R. Ooi, and K. Wódkiewicz, *Phys. Rev. Lett.* **96**, 010501 (2006).  
[18] A. A. Svidzinsky, J.-T. Chang, and M. O. Scully, *Phys. Rev. A* **81**, 053821 (2010).  
[19] T. Bienaimé, N. Piovella, and R. Kaiser, *Phys. Rev. Lett.* **108**, 123602 (2012).  
[20] J. Keaveney, A. Sargsyan, U. Krohn, I. G. Hughes, D. Sarkisyan, and C. S. Adams, *Phys. Rev. Lett.* **108**, 173601 (2012).  
[21] I. Sokolov, A. Kuraptsev, D. Kupriyanov, M. Havey, and S. Balik, *J. Mod. Opt.* **60**, 50 (2013).  
[22] J. Javanainen, J. Ruostekoski, Y. Li, and S.-M. Yoo, *Phys. Rev. Lett.* **112**, 113603 (2014).  
[23] I. Sokolov, *Laser Phys.* **25**, 065202 (2015).  
[24] R. Olave, A. Win, K. Kemp, S. Roof, S. Balik, M. Havey, I. Sokolov, and D. Kupriyanov, in *From Atomic to Mesoscale: The Role of Quantum Coherence in Systems of Various Complexities*, edited by S. A. Malinovskaya and I. Novikova (World Scientific, Singapore, 2015), pp. 39–59.  
[25] S. Jennewein, M. Besbes, N. J. Schilder, S. D. Jenkins, C. Sauvan, J. Ruostekoski, J.-J. Greffet, Y. R. P. Sortais, and A. Browaeys, *Phys. Rev. Lett.* **116**, 233601 (2016).  
[26] J. Javanainen and J. Ruostekoski, *Opt. Express* **24**, 993 (2016).  
[27] S. D. Jenkins, J. Ruostekoski, J. Javanainen, R. Bourgain, S. Jennewein, Y. R. P. Sortais, and A. Browaeys, *Phys. Rev. Lett.* **116**, 183601 (2016).  
[28] M. O. Araújo, I. Kresic, R. Kaiser, and W. Guerin, [arXiv:1603.07204](https://arxiv.org/abs/1603.07204).  
[29] P. C. Bons, R. de Haas, D. de Jong, A. Groot, and P. van der Straten, *Phys. Rev. Lett.* **116**, 173602 (2016).  
[30] B. Olmos, D. Yu, Y. Singh, F. Schreck, K. Bongs, and I. Lesanovsky, *Phys. Rev. Lett.* **110**, 143602 (2013).

- [31] T. Maier, S. Kraemer, L. Ostermann, and H. Ritsch, *Opt. Express* **22**, 13269 (2014).
- [32] D. Yu, *J. Mod. Opt.* **63**, 428 (2016).
- [33] B. Zhu, J. Schachenmayer, M. Xu, F. Herrera, J. G. Restrepo, M. J. Holland, and A. M. Rey, *New J. Phys.* **17**, 083063 (2015).
- [34] R. J. Bettles, S. A. Gardiner, and C. S. Adams, *Phys. Rev. A* **92**, 063822 (2015).
- [35] P. R. Berman, *Phys. Rev. A* **55**, 4466 (1997).
- [36] Q. Li, D. Xu, C. Cai, and C. Sun, *Sci. Rep.* **3**, 3144 (2013).
- [37] S. Jennewein, Y. Sortais, J.-J. Greffet, and A. Browaeys, [arXiv:1511.08527](https://arxiv.org/abs/1511.08527).
- [38] E. A. Goldschmidt, T. Boulier, R. C. Brown, S. B. Koller, J. T. Young, A. V. Gorshkov, S. L. Rolston, and J. V. Porto, *Phys. Rev. Lett.* **116**, 113001 (2016).
- [39] P. de Vries, D. V. van Coevorden, and A. Lagendijk, *Rev. Mod. Phys.* **70**, 447 (1998).
- [40] M. C. W. van Rossum and T. M. Nieuwenhuizen, *Rev. Mod. Phys.* **71**, 313 (1999).
- [41] G. Labeyrie, D. Delande, C. A. Müller, C. Miniatura, and R. Kaiser, *Phys. Rev. A* **67**, 033814 (2003).
- [42] W. Brown and K. Mortensen, *Scattering in Polymeric and Colloidal Systems* (Gordon and Breach, New York, 2000).
- [43] G. Labeyrie, F. de Tomasi, J.-C. Bernard, C. A. Müller, C. Miniatura, and R. Kaiser, *Phys. Rev. Lett.* **83**, 5266 (1999).
- [44] G. Labeyrie, D. Delande, C. A. Mueller, C. Miniatura, and R. Kaiser, *Opt. Commun.* **243**, 157 (2004).
- [45] O. Sigwarth, G. Labeyrie, T. Jonckheere, D. Delande, R. Kaiser, and C. Miniatura, *Phys. Rev. Lett.* **93**, 143906 (2004).
- [46] G. Labeyrie, D. Delande, R. Kaiser, and C. Miniatura, *Phys. Rev. Lett.* **97**, 013004 (2006).
- [47] L. Chomaz, L. Corman, T. Yefsah, R. Desbuquois, and J. Dalibard, *New J. Phys.* **14**, 055001 (2012).
- [48] D. Yu, *Phys. Rev. A* **89**, 063809 (2014).
- [49] T. Bienaimé, R. Bachelard, J. Chabé, M. Rouabah, L. Bellando, P. Courteille, N. Piovella, and R. Kaiser, *J. Mod. Opt.* **61**, 18 (2014).
- [50] R. T. Sutherland and F. Robicheaux, *Phys. Rev. A* **93**, 023407 (2016).
- [51] Y. Miroshnichenko, U. V. Poulsen, and K. Mølmer, *Phys. Rev. A* **87**, 023821 (2013).
- [52] Z. Meir, O. Schwartz, E. Shahmoon, D. Oron, and R. Ozeri, *Phys. Rev. Lett.* **113**, 193002 (2014).
- [53] S. L. Bromley, B. Zhu, M. Bishop, X. Zhang, T. Bothwell, J. Schachenmayer, T. L. Nicholson, R. Kaiser, S. F. Yelin, M. D. Lukin *et al.*, *Nat. Commun.* **7**, 11039 (2016).
- [54] S. Roof, K. Kemp, M. Havey, and I. Sokolov, [arXiv:1603.07268](https://arxiv.org/abs/1603.07268).
- [55] M. Gross and S. Haroche, *Phys. Rep.* **93**, 301 (1982).
- [56] R. Friedberg, S. Hartmann, and J. Manassah, *Phys. Lett. A* **40**, 365 (1972).
- [57] F. C. Spano and S. Mukamel, *J. Chem. Phys.* **91**, 683 (1989).
- [58] R. Röhlberger, K. Schlage, B. Sahoo, S. Couet, and R. Ruffer, *Science* **328**, 1248 (2010).
- [59] Note that around the  $\theta = \pi$  direction there is a small enhancement of  $\sim 2$  due to the coherent backward scattering [41].
- [60] A. Lagendijk and B. A. Van Tiggelen, *Phys. Rep.* **270**, 143 (1996).
- [61] R. Friedberg, S. Hartmann, and J. Manassah, *Phys. Rep.* **7**, 101 (1973).
- [62] S. Balik, A. L. Win, M. D. Havey, I. M. Sokolov, and D. V. Kupriyanov, *Phys. Rev. A* **87**, 053817 (2013).
- [63] Note that for a cloud with a Gaussian distribution, the size of the incident laser beam needs to be taken into account since a broad beam experiences fewer scattering events at the edge of the cloud and the actual optical depth depends on the transverse coordinates. The finite beam size is not taken into account in the CD presented here. In RW we choose the beam size to be 5 times the Gaussian width of the cloud.
- [64] J. Chabé, M.-T. Rouabah, L. Bellando, T. Bienaimé, N. Piovella, R. Bachelard, and R. Kaiser, *Phys. Rev. A* **89**, 043833 (2014).
- [65] M. J. Raković, G. W. Kattawar, M. Mehrübeoğlu, B. D. Cameron, L. V. Wang, S. Rastegar, and G. L. Coté, *Appl. Opt.* **38**, 3399 (1999).
- [66] J. Hovenier, C. Mee, and H. Domke, *Transfer of Polarized Light in Planetary Atmospheres: Basic Concepts and Practical Methods*, Astrophysics and Space Science Library (Springer, Berlin, 2004).
- [67] C. Brosseau, *Fundamentals of Polarized Light: A Statistical Optics Approach* (Wiley, New York, 1998).
- [68] S. Bartel and A. H. Hielscher, *Appl. Opt.* **39**, 1580 (2000).
- [69] T. Ido, T. H. Loftus, M. M. Boyd, A. D. Ludlow, K. W. Holman, and J. Ye, *Phys. Rev. Lett.* **94**, 153001 (2005).
- [70] M. Trippenbach, B. Gao, J. Cooper, and K. Burnett, *Phys. Rev. A* **45**, 6555 (1992).
- [71] W. D. Phillips, *Rev. Mod. Phys.* **70**, 721 (1998).
- [72] F. Damanet, D. Braun, and J. Martin, *Phys. Rev. A* **93**, 022124 (2016).
- [73] A. M. Smith and K. Burnett, *J. Opt. Soc. Am. B* **8**, 1592 (1991).
- [74] A. M. Smith and K. Burnett, *J. Opt. Soc. Am. B* **9**, 1240 (1992).
- [75] Y. Castin, H. Wallis, and J. Dalibard, *J. Opt. Soc. Am. B* **6**, 2046 (1989).
- [76] Note that the counterrotating terms such as  $\hat{a}_{\mathbf{k}\epsilon}\hat{b}$  have been dropped because the relevant states are restricted to include at most one excitation.
- [77] J. F. Lam and P. R. Berman, *Phys. Rev. A* **14**, 1683 (1976).